On the Convergence of the Classical Symmetrical Condensed Node–TLM Scheme

Jürgen N. Rebel, Martin Aidam, and Peter Russer, *Fellow, IEEE*

***Abstract*—This paper presents a proof of convergence of the transmission-line matrix (TLM) method with a symmetrical condensed node (SCN) in the classical formulation of Johns. It is shown that the convergence order of the SCN–TLM method cannot simply be derived from observing the dispersion characteristics of the TLM mesh. The mapping between the discretized electromagnetic field and TLM wave amplitudes plays a decisive role. Although second-order convergence is observed for coarse discretizations, which are usually used in practice due to the limitations of memory resources, it is shown and numerically verified that the asymptotic convergence reduces to order $\mathcal{O}(\sqrt{\Delta t})$. Only using a bijective field mapping defined at the cell boundaries yields second-order convergence.**

I. Introduction

ALTHOUGH the transmission-line matrix (TLM) algorithm with a symmetrical condensed node (SCN) in the formulation of Johns [1] has been applied to solve electromagnetic-field problems for many years, a proof of convergence of the method has yet to be given.

When Johns introduced the SCN–TLM scheme, he was guided by the analogy between the propagation of electromagnetic waves in free space and the propagation of current and voltage waves on an interconnected mesh of transmission lines. Therefore, various authors tried to find equivalent finite-difference formulations, which could be derived directly from Maxwell's equations. Due to the fact that there exists a large variety of techniques to derive difference operators, the authors went along these lines. Examples are the method-of-moments [2], Taylor-series expansion [3], [4], finite integration [5], and conservation law approaches [6].

However, there exists a different interpretation of the TLM algorithm using a discrete propagator integral, which leads to second-order convergence [7]. Nevertheless, the classical formulation of Johns is commonly used.

In this paper, we give a proof of the convergence of the classical formulation of Johns. This is done by showing that the TLM scheme converges against an equivalent finite-difference scheme induced by mapping the TLM wave pulses to the discretized electromagnetic field at each time step and subsequently exciting the TLM mesh anew by mapping the discretized electromagnetic field back to the wave pulses.

If the operating condition of the TLM scheme is altered in this way, one can derive a so-called *mapping-induced finite-difference scheme*, which can be assessed using standard techniques for proving consistency, stability, and convergence [8]. Here, we show the convergence of this scheme using Lax's theorem, which states that a consistent and stable difference scheme does converge. The mapping-induced finite-difference scheme is first-order accurate.

In a second step, we show that the distance between the mapping-induced finite-difference scheme and the original TLM scheme becomes arbitrarily small when the time step approaches zero. From this, the convergence of the TLM scheme in the formulation of Johns follows.

The predictions of the theory are verified by numerical experiments, which are presented in a following section.

II. Initial Boundary-Value Problem

Maxwell's equations are given on a bounded region $\boldsymbol{\Omega} \subset \mathbb{R}^3$ with boundary $\partial\boldsymbol{\Omega}$ for stationary media characterized by permittivity, permeability, and both electric and magnetic conductance by

$$\varepsilon\frac{\partial\vec{\boldsymbol{E}}}{\partial t} + \boldsymbol{\sigma}_e\vec{\boldsymbol{E}} = \nabla \times \vec{\boldsymbol{H}} \tag{1}$$

$$\boldsymbol{\mu}\frac{\partial\vec{\boldsymbol{H}}}{\partial t} + \boldsymbol{\sigma}_m\vec{\boldsymbol{H}} = -\nabla \times \vec{\boldsymbol{E}} \tag{2}$$

with appropriate initial values (IVs)

$$\vec{\boldsymbol{E}}(\vec{\boldsymbol{x}}, t=0) \quad \vec{\boldsymbol{H}}(\vec{\boldsymbol{x}}, t=0) \tag{3}$$

and appropriate boundary conditions

$$\vec{\boldsymbol{E}}(\partial\boldsymbol{\Omega}, t) \quad \vec{\boldsymbol{H}}(\partial\boldsymbol{\Omega}, t). \tag{4}$$

An appropriate function space for this initial value problem (IVP) is given by the Lebesgue space of square integrable functions [9]–[11]

$$\boldsymbol{L}_2\Big(0, T; \big(\boldsymbol{L}_2(\boldsymbol{\Omega})\big)^6\Big). \tag{5}$$

Manuscript received August 11, 1999. The work of J. N. Rebel and M. Aidam was supported by Siemens AG under an Ernst-von-Siemens Scholarship.

J. N. Rebel was with the Institut für Hochfrequenztechnik, Technische Universität München, D-80333 Munich, Germany. He is now with the Wireless Group, Infineon Technologies AG, D-81541 Munich, Germany.

M. Aidam was with the Institut für Hochfrequenztechnik, Technische Universität München, D-80333 Munich, Germany. He is now with Daimler Chrysler, D-71059 Sindelsingen, Germany.

P. Russer is with the Institut für Hochfrequenztechnik, Technische Universität München, D-80333 Munich, Germany.

Publisher Item Identifier S 0018-9480(01)03321-X.

III. Mapping-Induced Finite-Difference Schemes of TLM–SCN Schemes

Using the notation following [12], we identify the hitherto axiomatic Hilbert space $\mathcal{H}_w$ with the discrete Lebesgue space analogously to (5)

$$\ell_{2,\Delta t}\Big(\{k\};\big(\ell_{2,\Delta x,\Delta y,\Delta z}(\boldsymbol{G})\big)^q\Big) \tag{6}$$

where the integer set $\{k\}$ denotes the discrete time interval, q is the appropriate dimension, i.e., 12 for the SCN without stubs and 18 for the TLM scheme with stubs. The grid of discrete points where the electromagnetic field is sampled, i.e., the location of the TLM nodes, is denoted by $\boldsymbol{G} \subset \boldsymbol{\Omega}$. The norm in this space is defined by [8], [10]

$$|||u\rangle||_{\mathcal{H}_w} = \sqrt{\sum_k |||_k u\rangle||^2_{\ell_{2,\Delta x,\Delta y,\Delta z}} \Delta t} \tag{7}$$

with

$$|||_k u\rangle||^2_{\ell_{2,\Delta x,\Delta y,\Delta z}} = \sqrt{\sum_{\boldsymbol{l},m,n,j} |u^j_{\boldsymbol{l},m,n}|^2 \Delta x \Delta y \Delta z} \tag{8}$$

and

$$|u\rangle = \sum_{k,\boldsymbol{l},m,n} \boldsymbol{u}_{k;\boldsymbol{l},m,n} |k;l,m,n\rangle \tag{9}$$

with $\boldsymbol{u}_{k;\boldsymbol{l},m,n} = [u^1_{k;\boldsymbol{l},m,n},\ldots,u^j_{k;\boldsymbol{l},m,n}]^{\mathrm{T}}$.

Briefly recalling the ket vectors[1] of incident and reflected wave pulses

$$|a\rangle = \sum_{k,\boldsymbol{l},m,n} \boldsymbol{a}_{k;\boldsymbol{l},m,n} |k;l,m,n\rangle \tag{10}$$

$$|b\rangle = \sum_{k,\boldsymbol{l},m,n} \boldsymbol{b}_{k;\boldsymbol{l},m,n} |k;l,m,n\rangle \tag{11}$$

with $\boldsymbol{a}_{k;\boldsymbol{l},m,n} = [a^1_{k;\boldsymbol{l},m,n},\ldots,a^q_{k;\boldsymbol{l},m,n}]^{\mathrm{T}}$ and $\boldsymbol{b}_{k;\boldsymbol{l},m,n}$ analogously, and the ket vector of field state

$$|f\rangle = \sum_{k,\boldsymbol{l},m,n} \boldsymbol{f}_{k;\boldsymbol{l},m,n} |k;l,m,n\rangle \tag{12}$$

with $\boldsymbol{f}_{k;\boldsymbol{l},m,n} = [E^x,E^y,E^z,Z_0H^x,Z_0H^y,Z_0H^z]^{\mathrm{T}}_{k;\boldsymbol{l},m,n}$. The scattering and connection operators are given by

$$\boldsymbol{S} = \sum_{\boldsymbol{l},m,n} |l,m,n\rangle \boldsymbol{S}_{\boldsymbol{l},m,n} \langle l,m,n| \tag{13}$$

$$\boldsymbol{\Gamma} = \sum_{\boldsymbol{l},m,n} |l,m,n\rangle \boldsymbol{\Gamma}_{\boldsymbol{l},m,n} \langle l,m,n|. \tag{14}$$

$\boldsymbol{S}_{\boldsymbol{l},m,n}$ and $\boldsymbol{\Gamma}_{\boldsymbol{l},m,n}$ are shown in Figs. 1 and 2 for the formulation with stubs, and denote the local scattering and connection operators in their matrix representation [for the formulation without stubs, refer to (23) and (25)]. In the sequel, the indexes l,m,n for denoting local operators are omitted. The TLM algorithm is characterized by the two operations scattering and connecting

$$|b\rangle = \boldsymbol{T}\boldsymbol{S}|a\rangle \tag{15}$$

$$|a\rangle = \boldsymbol{\Gamma}|b\rangle. \tag{16}$$

$\boldsymbol{T}$ denotes the time-shift operator, i.e., $\boldsymbol{T}|k\rangle = |k+1\rangle$. Inserting (15) into (16) yields a finite-difference scheme in the incident TLM wave amplitudes $\boldsymbol{a}_{k;\boldsymbol{l},m,n}$ (the operator $\boldsymbol{T}$ commutes with the operators $\boldsymbol{\Gamma}$ and $\boldsymbol{S}$)

$$|a\rangle = \boldsymbol{T}\boldsymbol{\Gamma}\boldsymbol{S}|a\rangle. \tag{17}$$

The idea of writing the TLM algorithm as an equivalent finite-difference scheme involves the mapping of the TLM operator to the equivalent difference operator for each time step. Consequently, the operation conditions are altered such that before each scattering event, the TLM state variables are mapped to the discretized field components and immediately mapped

[1]The term ket vector has been introduced by Dirac [13]

Column No.	1	2	3	4	5	6	7	8	9	10	11	12	13	14	15	16	17	18
o/c Stub (Y)	y	y	z	z	z	z	x	x	x	x	y	y	x	y	z			
s/c Stub (Z)	z	z	y	y	x	x	z	z	y	y	x	x				x	y	z
1	y	z	a	c			d	-d			b	b		g				-d
2	y	z	c	a			-d	d			b	b		g				d
3	z	y			a	c	b	b		d	-d				g		d	
4	z	y			c	a	b	b		-d	d				g		-d	
5	z	x			b	b	a	c				d	-d			g	-d	
6	z	x			b	b	c	a				-d	d			g	d	
7	x	z	d	-d				a	c	b	b			g				d
8	x	z	-d	d				c	a	b	b			g				-d
9	x	y			d	-d		b	b	a	c			g			-d	
10	x	y			-d	d		b	b	c	a			g			d	
11	y	x	b	b			d	-d				a	c		g		d	
12	y	x	b	b			-d	d				c	a		g		-d	
13	x							b	b	b	b			h				
14	y		b	b							b	b			h			
15	z				b	b	b	b								h		
16		x					-f	f				f	-f				j	
17		y			f	-f				-f	f							j
18		z	-f	f				f	-f										j
Row (Y) (Z)																		

Fig. 1. Scattering matrix with stubs.

Port	1	2	3	4	5	6	7	8	9	10	11	12	13	14	15	16	17	18
1		$\boldsymbol{X}$																
2	$\boldsymbol{X}^\dagger$																	
3				$\boldsymbol{X}$														
4			$\boldsymbol{X}^\dagger$															
5						$\boldsymbol{Y}$													
6					$\boldsymbol{Y}^\dagger$													
7								$\boldsymbol{Y}$										
8							$\boldsymbol{Y}^\dagger$											
9										$\boldsymbol{Z}$								
10									$\boldsymbol{Z}^\dagger$									
11												$\boldsymbol{Z}$						
12											$\boldsymbol{Z}^\dagger$							
13													1					
14														1				
15															1			
16																-1		
17																	-1	
18																		-1

Fig. 2. Extended connection operator.

back to the TLM state variables. The field and wave amplitudes are related by

$$|a\rangle = \boldsymbol{Q}|f\rangle \tag{18}$$
$$|f\rangle = \boldsymbol{P}|a\rangle. \tag{19}$$

Applying the mapping operator $\boldsymbol{P}$ from the left-hand side to (17) and substituting (19) on the right-hand side of (17) consequently results in the *mapping-induced finite-difference scheme*

$$|f\rangle = \boldsymbol{PT\Gamma SQ}|f\rangle \tag{20}$$

or

$$\sum_k |_k f\rangle = \sum_k \boldsymbol{P\Gamma SQ}|_k f\rangle \tag{21}$$

better showing the nature of a finite-difference scheme. As

$$\boldsymbol{QP} \neq \boldsymbol{I} \tag{22}$$

holds [2] ($\boldsymbol{I}$ denoting the identity operator), one has to consider the differences between the mapping-induced finite-difference scheme and the classical TLM scheme before one can draw conclusions on the properties of one scheme from the properties of the other scheme.

However, we will show in the following sections that the solutions provided by this mapping-induced finite-difference scheme converge against solutions of Maxwell's equations using Lax's theorem and that we can indeed draw conclusions on the behavior of the SCN–TLM scheme.

IV. Mapping-Induced Finite-Difference Scheme of TLM without Stubs

First, we want to look at the stubfree formulation. The scattering matrix without stubs is given by

$$\boldsymbol{S} = \begin{pmatrix} \boldsymbol{0} & \boldsymbol{S}_0 & \boldsymbol{S}_0^{\mathrm{T}} \\ \boldsymbol{S}_0^{\mathrm{T}} & \boldsymbol{0} & \boldsymbol{S}_0 \\ \boldsymbol{S}_0 & \boldsymbol{S}_0^{\mathrm{T}} & \boldsymbol{0} \end{pmatrix} \tag{23}$$

with

$$\boldsymbol{S}_0 = \begin{pmatrix} 0 & 0 & \frac{1}{2} & -\frac{1}{2} \\ 0 & 0 & -\frac{1}{2} & \frac{1}{2} \\ \frac{1}{2} & \frac{1}{2} & 0 & 0 \\ \frac{1}{2} & \frac{1}{2} & 0 & 0 \end{pmatrix}. \tag{24}$$

The connection operator $\boldsymbol{\Gamma}$ writes in matrix representation

$$\boldsymbol{\Gamma} = \begin{pmatrix} \boldsymbol{A(X)} & \boldsymbol{0} & \boldsymbol{0} \\ \boldsymbol{0} & \boldsymbol{A(Y)} & \boldsymbol{0} \\ \boldsymbol{0} & \boldsymbol{0} & \boldsymbol{A(Z)} \end{pmatrix} \tag{25}$$

with

$$\boldsymbol{A(X)} = \begin{pmatrix} 0 & \boldsymbol{X} & 0 & 0 \\ \boldsymbol{X}^\dagger & 0 & 0 & 0 \\ 0 & 0 & 0 & \boldsymbol{X} \\ 0 & 0 & \boldsymbol{X}^\dagger & 0 \end{pmatrix}. \tag{26}$$

$\boldsymbol{X}^\dagger$ denotes the Hermitian conjugate of $\boldsymbol{X}$. The operator $\boldsymbol{X}^\dagger$ decrements the index l by one. The mapping between field and wave amplitudes is given by

$$\boldsymbol{P} = \boldsymbol{Q}^{\mathrm{T}} = \frac{1}{2} \begin{pmatrix} 0 & 1 & 0 & 0 & 0 & 1 \\ 0 & 1 & 0 & 0 & 0 & -1 \\ 0 & 0 & 1 & 0 & -1 & 0 \\ 0 & 0 & 1 & 0 & 1 & 0 \\ 0 & 0 & 1 & 1 & 0 & 0 \\ 0 & 0 & 1 & -1 & 0 & 0 \\ 1 & 0 & 0 & 0 & 0 & -1 \\ 1 & 0 & 0 & 0 & 0 & 1 \\ 1 & 0 & 0 & 0 & 1 & 0 \\ 1 & 0 & 0 & 0 & -1 & 0 \\ 0 & 1 & 0 & -1 & 0 & 0 \\ 0 & 1 & 0 & 1 & 0 & 0 \end{pmatrix}^{\mathrm{T}}. \tag{27}$$

According to (21) and (23)–(27), we get

$$\boldsymbol{P\Gamma SQ} = \frac{1}{4} \begin{pmatrix} \boldsymbol{D}_{YZ} & 0 & 0 & 0 & -\boldsymbol{D}_Z & \boldsymbol{D}_Y \\ 0 & \boldsymbol{D}_{XZ} & 0 & \boldsymbol{D}_Z & 0 & -\boldsymbol{D}_X \\ 0 & 0 & \boldsymbol{D}_{XY} & -\boldsymbol{D}_Y & \boldsymbol{D}_X & 0 \\ 0 & \boldsymbol{D}_Z & -\boldsymbol{D}_Y & \boldsymbol{D}_{YZ} & 0 & 0 \\ -\boldsymbol{D}_Z & 0 & \boldsymbol{D}_X & 0 & \boldsymbol{D}_{XZ} & 0 \\ \boldsymbol{D}_Y & -\boldsymbol{D}_X & 0 & 0 & 0 & \boldsymbol{D}_{XY} \end{pmatrix} \tag{28}$$

with

$$\begin{aligned} \boldsymbol{D}_X &= \boldsymbol{X}^\dagger - \boldsymbol{X} \\ \boldsymbol{D}_{XY} &= \boldsymbol{X}^\dagger + \boldsymbol{X} + \boldsymbol{Y}^\dagger + \boldsymbol{Y} \\ \boldsymbol{D}_Y &= \boldsymbol{Y}^\dagger - \boldsymbol{Y} \\ \boldsymbol{D}_{XZ} &= \boldsymbol{X}^\dagger + \boldsymbol{X} + \boldsymbol{Z}^\dagger + \boldsymbol{Z} \\ \boldsymbol{D}_Z &= \boldsymbol{Z}^\dagger - \boldsymbol{Z} \\ \boldsymbol{D}_{YZ} &= \boldsymbol{Y}^\dagger + \boldsymbol{Y} + \boldsymbol{Z}^\dagger + \boldsymbol{Z}. \end{aligned}$$

A. Consistency of Mapping-Induced Finite-Difference Scheme

To prove consistency, we expand the sampled exact continuous solution of the Maxwell's equations at the point $(k;l,m,n)$ in a Taylor series, insert this expanded solution into the finite-difference scheme, and let $\Delta t \longrightarrow 0$ and $\Delta l \longrightarrow 0$, which should yield the desired partial differential equation [8]. Writing each component, this yields the following mapping-induced finite-difference scheme:[2]

$$\begin{aligned} {}_{k+1}E^x_{l,m,n} =& \frac{1}{4}\Big({}_kE^x_{l,m+1,n} + {}_k E^x_{l,m-1,n} \\ &+ {}_k E^x_{l,m,n+1} + {}_k E^x_{l,m,n-1}\Big) \\ &- \frac{1}{\varepsilon_0}\frac{\Delta t}{2\Delta l}\Big({}_kH^y_{l,m,n+1} - {}_k H^y_{l,m,n-1}\Big) \\ &+ \frac{1}{\varepsilon_0}\frac{\Delta t}{2\Delta l}\Big({}_kH^z_{l,m+1,n} - {}_k H^z_{l,m-1,n}\Big). \end{aligned} \tag{29}$$

However, this is exactly the well-known Lax–Friedrichs finite-difference scheme [8].

[2]In the case of a TLM without stubs, we only want to look at the x-component of Ampère's law. The other equations follow by symmetry and duality.

Expanding E^x, H^y, and H^z in a Taylor series and inserting into (29) yields

$$\begin{aligned}\varepsilon_0\frac{\partial E^x}{\partial t}\Big|_{l\Delta l,m\Delta l,n\Delta l;k\Delta t}&+\mathcal{O}(\Delta t)+\mathcal{O}\left(\frac{\Delta l^2}{\Delta t}\right)\\&=-\frac{\partial H^y}{\partial z}\Big|_{l\Delta l,m\Delta l,n\Delta l;k\Delta t}+\mathcal{O}(\Delta l^2)\\&\quad+\frac{\partial H^z}{\partial y}\Big|_{l\Delta l,m\Delta l,n\Delta l;k\Delta t}+\mathcal{O}(\Delta l^2).\end{aligned}\tag{30}$$

As expected from a Lax–Friedrichs scheme, the inherent mapping-induced finite-difference scheme of the classical free-space TLM is first-order accurate in time and $\mathcal{O}(\Delta l^2)$ in space.

V. Mapping-Induced Finite-Difference Scheme of TLM with Stubs

We now want to analyze the mapping-induced finite-difference scheme of the SCN–TLM scheme with stubs in the formulation of Johns [1]. When ohmic and magnetic losses are included, we consider the extensions proposed by Naylor and Desai [14]. For calculating $\boldsymbol{P\Gamma SQ}$, as in (28), $\boldsymbol{P}$, $\boldsymbol{\Gamma}$, $\boldsymbol{S}$, and $\boldsymbol{Q}$ are given as follows.

If both electric and magnetic losses need to be considered, the matrix elements a,b,c,d,f,g,h,j of the scattering matrix shown in Fig. 1 calculate

$$\begin{aligned}a&=-\frac{G+Y}{2(G+Y+4)}+\frac{R+Z}{2(R+Z+4)}\\c&=-\frac{G+Y}{2(G+Y+4)}-\frac{R+Z}{2(R+Z+4)}\\b&=\frac{2}{G+Y+4}\\d&=\frac{2}{Z+R+4}\\g&=\frac{2Y}{G+Y+4}\\f&=\frac{2Z}{R+Z+4}\\h&=-\frac{G-Y+4}{G+Y+4}\\j&=\frac{4-Z+R}{R+Z+4}.\end{aligned}\tag{31}$$

With graded space discretization $u\Delta l, v\Delta l, w\Delta l$, the material parameters Y,Z,R,G are given by

$$\begin{aligned}Y_x&=2\left(\frac{vw}{u}\varepsilon_r' h-2\right)\\Z_x&=2\left(\frac{vw}{u}\mu_r' h-2\right)\\Y_y&=2\left(\frac{uw}{v}\varepsilon_r' h-2\right)\\Z_y&=2\left(\frac{uw}{v}\mu_r' h-2\right)\\Y_z&=2\left(\frac{uv}{w}\varepsilon_r' h-2\right)\\Z_z&=2\left(\frac{uv}{w}\mu_r' h-2\right)\\G_x&=\frac{vw}{u}\sigma_{ex}\Delta l Z_0\\R_x&=\frac{vw}{u}\sigma_{mx}\frac{\Delta l}{Z_0}\\G_y&=\frac{uw}{v}\sigma_{ey}\Delta l Z_0\\R_y&=\frac{uw}{v}\sigma_{my}\frac{\Delta l}{Z_0}\\G_z&=\frac{uv}{w}\sigma_{ez}\Delta l Z_0\\R_z&=\frac{uv}{w}\sigma_{mz}\frac{\Delta l}{Z_0}.\end{aligned}\tag{32}$$

The dashed permittivities and permeabilities are the physical permittivities and permeabilities of the medium scaled by a constant factor. The reason for this will become evident later. The stability factor of the TLM scheme h is given by $h_0\Delta l/c_0\Delta t$. h_0 is the factor by which the speed of light is scaled in the TLM mesh. The extended connection operator writes in matrix form, as shown in Fig. 2. The mapping between field and wave amplitudes is given by

$$\boldsymbol{P}=\begin{pmatrix}0&b_y&0&0&0&d_z\\0&b_y&0&0&0&-d_z\\0&0&b_z&0&-d_y&0\\0&0&b_z&0&d_y&0\\0&0&b_z&d_x&0&0\\0&0&b_z&-d_x&0&0\\b_x&0&0&0&0&-d_z\\b_x&0&0&0&0&d_z\\b_x&0&0&0&d_y&0\\b_x&0&0&0&-d_y&0\\0&b_y&0&-d_x&0&0\\0&b_y&0&d_x&0&0\\b_xY_x&0&0&0&0&0\\0&b_yY_y&0&0&0&0\\0&0&b_zY_z&0&0&0\\0&0&0&-d_x&0&0\\0&0&0&0&-d_y&0\\0&0&0&0&0&-d_z\end{pmatrix}^{\mathrm{T}}\tag{33}$$

with the coefficients

$$\begin{aligned}b_x&=\frac{2}{u(G_x+Y_x+4)}\\d_x&=\frac{2}{u(R_x+Z_x+4)}\\b_y&=\frac{2}{v(G_y+Y_y+4)}\\d_y&=\frac{2}{v(R_y+Z_y+4)}\\b_z&=\frac{2}{w(G_z+Y_z+4)}\\d_z&=\frac{2}{w(R_z+Z_z+4)}.\end{aligned}\tag{34}$$

Excitation of the TLM-SCN network is performed by the following mapping

$$\boldsymbol{Q}=\frac{1}{2}\begin{pmatrix} 0 & v & 0 & 0 & 0 & -w \\ 0 & v & 0 & 0 & 0 & w \\ 0 & 0 & w & 0 & v & 0 \\ 0 & 0 & w & 0 & -v & 0 \\ 0 & 0 & w & -u & 0 & 0 \\ 0 & 0 & w & u & 0 & 0 \\ u & 0 & 0 & 0 & 0 & w \\ u & 0 & 0 & 0 & 0 & -w \\ u & 0 & 0 & 0 & -v & 0 \\ u & 0 & 0 & 0 & v & 0 \\ 0 & v & 0 & u & 0 & 0 \\ 0 & v & 0 & -u & 0 & 0 \\ ua_x & 0 & 0 & 0 & 0 & 0 \\ 0 & va_y & 0 & 0 & 0 & 0 \\ 0 & 0 & wa_z & 0 & 0 & 0 \\ 0 & 0 & 0 & -uc_x & 0 & 0 \\ 0 & 0 & 0 & 0 & -vc_y & 0 \\ 0 & 0 & 0 & 0 & 0 & -wc_z \end{pmatrix} \tag{35}$$

with the coefficients

$$\begin{aligned} a_x =& \frac{Y_x+G_x}{Y_x} \\ c_x =& (Z_x+R_x) \\ a_y =& \frac{Y_y+G_y}{Y_y} \\ c_y =& (Z_y+R_y) \\ a_z =& \frac{Y_z+G_z}{Y_z} \\ c_z =& (Z_z+R_z). \end{aligned} \tag{36}$$

It should be remarked that the coefficients are slightly different in comparison to [14]. Only with these modifications, the mapping-induced finite-difference scheme derived from the TLM scheme given in [14] is consistent with Maxwell's equations.

A. Consistency

Again, to prove consistency, we expand the sampled exact continuous solution of the Maxwell's equations at the point $(k;l,m,n)$ in a Taylor series, insert this expanded solution into the finite-difference scheme, and let $\Delta t \longrightarrow 0$ and $\Delta l \longrightarrow 0$. We only want to look at the x-component of both Ampère's and Faraday's laws. The other equations follow by symmetry. For simplicity, we set $\Delta x = u\Delta l$, $\Delta y = v\Delta l$, and $\Delta z = w\Delta l$ in the sequel.

B. Mapping-Induced Finite-Difference Scheme of Johns' Matrix Without Losses

Evaluating (21) for both $\boldsymbol{\sigma}_e = \mathbf{o}$ and $\boldsymbol{\sigma}_m = \mathbf{o}$ yields the following finite-difference scheme, i.e., for the x-component of Ampère's law

$$\begin{aligned} {}_{k+1}E^x_{l,m,n} =& {}_k E^x_{l,m,n} + \frac{u}{w}\frac{r_{xy}}{2Z_0}({}_kE^x_{l,m+1,n} - 2{}_kE^x_{l,m,n} + {}_k E^x_{l,m-1,n}) \\ &+ \frac{u}{v}\frac{r_{xz}}{2Z_0}({}_kE^x_{l,m,n+1} - 2{}_kE^x_{l,m,n} + {}_k E^x_{l,m,n-1}) \\ &- \frac{r_{xz}}{2}({}_kH^y_{l,m,n+1} - {}_k H^y_{l,m,n-1}) \\ &+ \frac{r_{xy}}{2}({}_kH^z_{l,m+1,n} - {}_k H^z_{l,m-1,n}), \end{aligned} \tag{37}$$

with the stability factor of the mapping-induced finite-difference scheme

$$r_{xy} = \frac{1}{\varepsilon_0 h_0 \varepsilon_{rx}}\frac{\Delta t}{\Delta y}. \tag{38}$$

The other stabiltiy factors of the mapping-induced finite-difference scheme are defined analogously. For the x-component of Faraday's law, one gets

$$\begin{aligned} {}_{k+1}H^x_{l,m,n} =& {}_k H^x_{l,m,n} + \frac{u}{w}\frac{Z_0 r^*_{xy}}{2}\Big({}_kH^x_{l,m+1,n} - 2{}_kH^x_{l,m,n} \\ &+ {}_k H^x_{l,m-1,n}\Big) \\ &+ \frac{u}{v}\frac{Z_0 r^*_{xz}}{2}\Big({}_kH^x_{l,m,n+1} - 2{}_kH^x_{l,m,n} + {}_k H^x_{l,m,n-1}\Big) \\ &+ \frac{r^*_{xz}}{2}\Big({}_kE^y_{l,m,n+1} - {}_k E^y_{l,m,n-1}\Big) \\ &- \frac{r^*_{xy}}{2}\Big({}_kE^z_{l,m+1,n} - {}_k E^z_{l,m-1,n}\Big) \end{aligned} \tag{39}$$

where the stability factors of the mapping-induced finite-difference scheme are defined according to

$$r^*_{xy} = \frac{1}{\mu_0 h_0 \mu_{rx}}\frac{\Delta t}{\Delta y}. \tag{40}$$

Looking more closely at (37) and (39), one recognizes a forward-in-time–centered-in-space (FTCS) scheme, which is stabilized by adding artificial dispersion due to the $({}_kH^x_{l,m+1,n} - 2{}_kH^x_{l,m,n} + {}_k H^x_{l,m-1,n})$ and $({}_kE^x_{l,m+1,n} - 2{}_kE^x_{l,m,n} + {}_k E^x_{l,m-1,n})$ terms [8].

Expanding the sampled exact solution in a Taylor series, yields for Ampère's law

$$\begin{aligned} h_0\varepsilon'_{rx}\varepsilon_0\frac{\partial E^x}{\partial t}\Big|_{l\Delta x,m\Delta y,n\Delta z;k\Delta t} + \mathcal{O}(\Delta t) &= -\frac{\partial H^y}{\partial z}\Big|_{l\Delta x,m\Delta y,n\Delta z;k\Delta t} + \mathcal{O}(\Delta z^2) \\ &+ \frac{\partial H^z}{\partial y}\Big|_{l\Delta x,m\Delta y,n\Delta z;k\Delta t} + \mathcal{O}(\Delta y^2) \end{aligned} \tag{41}$$

and for Faraday's law

$$\begin{aligned} h_0\mu'_{rx}\mu_0\frac{\partial H^x}{\partial t}\Big|_{l\Delta x,m\Delta y,n\Delta z;k\Delta t} + \mathcal{O}(\Delta t) &= \frac{\partial E^y}{\partial z}\Big|_{l\Delta x,m\Delta y,n\Delta z;k\Delta t} + \mathcal{O}(\Delta z^2) \\ &- \frac{\partial E^z}{\partial y}\Big|_{l\Delta x,m\Delta y,n\Delta z;k\Delta t} + \mathcal{O}(\Delta y^2). \end{aligned} \tag{42}$$

As a consequence, the complete scheme is accurate of the order $\mathcal{O}(\Delta t) + \mathcal{O}(\Delta x^2) + \mathcal{O}(\Delta y^2) + \mathcal{O}(\Delta z^2)$.

Letting $\Delta t \longrightarrow 0$ and $\Delta l \longrightarrow 0$, the higher order terms vanish, and we are left with

$$h_0\varepsilon'_{rx}\varepsilon_0\frac{\partial E^x}{\partial t} = -\frac{\partial H^y}{\partial z} + \frac{\partial H^z}{\partial y} \tag{43}$$

and

$$h_0\mu'_{rx}\mu_0\frac{\partial H^x}{\partial t} = \frac{\partial E^y}{\partial z} - \frac{\partial E^z}{\partial y} \tag{44}$$

which is the desired partial differential equation, except for both dashed permittivity and permeability being scaled by h_0. Consequently, the relation between physical media parameters and TLM media parameters is given by

$$\varepsilon_r = h_0\varepsilon'_r \quad \mu_r = h_0\mu'_r. \tag{45}$$

Hence, if the mapping-induced finite-difference TLM scheme is supposed to simulate a physical medium with permittivity and permeability, its corresponding TLM media parameters in the stubs (32) have to be scaled by h_0 in accordance with (45). The reason for this is that the propagation velocity in the TLM mesh is given by the product of h_0 and the plane-wave propagation velocity of the medium to be modeled. In case of a TLM without stubs, the higher propagation velocity of in the TLM mesh could be seen as a result of the inherent Lax–Friedrichs scheme of the mapping-induced finite-difference scheme.

C. Mapping-Induced Finite-Difference Scheme of Johns' Matrix with Losses

To illustrate how a mapping-induced finite-difference scheme following (20) and (21) looks as if we include losses, we consider the case with ohmic losses. Considering both ohmic and magnetic losses would yield a scheme with a large number of terms, and its representation would only blur the main idea.

Considering only ohmic losses, the mapping-induced finite-difference scheme writes

$$\begin{aligned}{}_{k+1}E^x_{l,m,n} =& \frac{2(\varepsilon_0 h_0\varepsilon'_{rx})^2 - \Delta t\sigma_{ex}^2}{2(\varepsilon_0 h_0\varepsilon'_{rx})^2 + 2\varepsilon_0\varepsilon'_{rx}\sigma_{ex} + \Delta t\sigma_{ex}^2}\,{}_kE^x_{l,m,n} \\ &+ \frac{u}{w}\frac{r_{xy}}{2Z_0}\Big({}_kE^x_{l,m+1,n} - 2{}_kE^x_{l,m,n} + {}_kE^x_{l,m-1,n}\Big) \\ &+ \frac{u}{v}\frac{r_{xz}}{2Z_0}\Big({}_kE^x_{l,m,n+1} - 2{}_kE^x_{l,m,n} + {}_kE^x_{l,m,n-1}\Big) \\ &- \frac{r_{xz}}{2}\Big({}_kH^y_{l,m,n+1} - {}_kH^y_{l,m,n-1}\Big) \\ &+ \frac{r_{xy}}{2}\Big({}_kH^z_{l,m+1,n} - {}_kH^z_{l,m-1,n}\Big)\end{aligned} \tag{46}$$

with the stability factors of this mapping-induced finite-difference scheme given by

$$r_{xy} = \frac{2h_0\varepsilon_0\varepsilon'_{rx} + \sigma_{ex}\Delta t}{2(\varepsilon_0 h_0\varepsilon'_{rx})^2 + 2\varepsilon_0\varepsilon'_{rx}\sigma_{ex} + \Delta t\sigma_{ex}^2}\frac{\Delta t}{\Delta y} \tag{47}$$

and for Faradays law

$$\begin{aligned}{}_{k+1}H^x_{l,m,n} =& {}_kH^x_{l,m,n} + \frac{u}{w}\frac{Z_0 r^*_{xy}}{2}\Big({}_kH^x_{l,m+1,n} - 2{}_kH^x_{l,m,n} + {}_kH^x_{l,m-1,n}\Big) \\ &+ \frac{u}{v}\frac{Z_0 r^*_{xz}}{2}\Big({}_kH^x_{l,m,n+1} - 2{}_kH^x_{l,m,n} + {}_kH^x_{l,m,n-1}\Big) \\ &+ \frac{r^*_{xz}}{2}\Big({}_kE^y_{l,m,n+1} - {}_kE^y_{l,m,n-1}\Big) \\ &- \frac{r^*_{xy}}{2}\Big({}_kE^z_{l,m+1,n} - {}_kE^z_{l,m-1,n}\Big)\end{aligned} \tag{48}$$

with the stability factors of the mapping-induced finite-difference scheme defined according to

$$r^*_{xy} = \frac{1}{\mu_0 h_0\mu_{rx}}\frac{\Delta t}{\Delta y}. \tag{49}$$

In (48), we can recognize again the FTCS scheme with added artificial dispersion, as in (39). The scheme considering ohmic losses (46) is of the same type, whereas the *forward-in-time* term is modified to account for the losses.

A Taylor series expansion of the sampled exact solution results for Ampère's law in

$$\begin{aligned}& h_0\varepsilon_0\varepsilon'_{rx}\frac{\partial E^x}{\partial t}\Big|_{l\Delta x,m\Delta y,n\Delta z;k\Delta t} + \mathcal{O}(\Delta t) \\ &\quad + \sigma_{ex}E^x\Big|_{l\Delta x,m\Delta y,n\Delta z;k\Delta t} + \mathcal{O}(\Delta t) \\ &\quad = -\frac{\partial H^y}{\partial z}\Big|_{l\Delta x,m\Delta y,n\Delta z;k\Delta t} + \mathcal{O}(\Delta t) + \mathcal{O}\big(\Delta z^2\big) \\ &\quad + \frac{\partial H^z}{\partial y}\Big|_{l\Delta x,m\Delta y,n\Delta z;k\Delta t} + \mathcal{O}(\Delta t) + \mathcal{O}\big(\Delta y^2\big)\end{aligned} \tag{50}$$

and for Faraday's law results in

$$\begin{aligned}& h_0\mu_0\mu'_{rx}\frac{\partial H^x}{\partial t}\Big|_{l\Delta x,m\Delta y,n\Delta z;k\Delta t} + \mathcal{O}(\Delta t) \\ &\quad = \frac{\partial E^y}{\partial z}\Big|_{l\Delta x,m\Delta y,n\Delta z;k\Delta t} + \mathcal{O}(\Delta t) + \mathcal{O}\big(\Delta z^2\big) \\ &\quad - \frac{\partial E^z}{\partial y}\Big|_{l\Delta x,m\Delta y,n\Delta z;k\Delta t} + \mathcal{O}(\Delta t) + \mathcal{O}\big(\Delta y^2\big).\end{aligned} \tag{51}$$

Hence, the complete scheme (all six components) is accurate of the order $\mathcal{O}(\Delta t)$, as the spatial derivatives have also associated with them higher order terms of the order $\mathcal{O}(\Delta t)$. Letting

$\Delta t \longrightarrow 0$ and $\Delta l \longrightarrow 0$, the higher order terms vanish, and we are left with the first component of Ampère's law

$$h_0 \varepsilon'_{rx} \varepsilon_0 \frac{\partial E^x}{\partial t} + \sigma_{ex} E^x = -\frac{\partial H^y}{\partial z} + \frac{\partial H^z}{\partial y} \tag{52}$$

and

$$h_0 \mu'_{rx} \mu_0 \frac{\partial H^x}{\partial t} = \frac{\partial E^y}{\partial z} - \frac{\partial E^z}{\partial y} \tag{53}$$

except that the relative dashed permittivity and permeability are again scaled by h_0, as in (43) and (44). Consequently, the physical permittivities and permeabilities are scaled, as in (45), which is, again, a consequence of the propagation velocity in the TLM mesh.

VI. Stability of Mapping-Induced Finite-Difference Schemes of TLM–SCN Schemes

To satisfy Lax's theorem, we need to show that the mapping-induced finite-difference scheme of the SCN is stable.

One way of showing stability is to apply a discrete Fourier transform in the spatial variables to $\boldsymbol{P\Gamma SQ}$ and show that the eigenvalues are bounded by one [8]. As one can only, in special cases, calculate the eigenvalues of square matrices of order greater than five analytically, we have to follow a different argument.

It is a matter of fact that if

$$|Y_x| \geq 0 \wedge |Y_y| \geq 0 \wedge |Y_z| \geq 0 \tag{54}$$

$$|Z_x| \geq 0 \wedge |Z_y| \geq 0 \wedge |Z_z| \geq 0 \tag{55}$$

is fulfilled, the TLM algorithm is stable. As $\boldsymbol{S}$ is unitary, it is also bounded [15]. $\boldsymbol{\Gamma}$ is a shift operator, therefore, it is isometric [15] and, hence, there exists an upper bound for the operator norm of $\boldsymbol{\Gamma S}$[3]

$$||\boldsymbol{\Gamma S}|| \leq C_1. \tag{56}$$

We essentially want to show that

$$||\boldsymbol{\Gamma S}|| \leq C_1 \Longrightarrow ||\boldsymbol{P\Gamma SQ}|| \leq C_2. \tag{57}$$

which is equivalent to

$$||\boldsymbol{P\Gamma SQ}|| \leq ||\boldsymbol{P}||||\boldsymbol{\Gamma S}||||\boldsymbol{Q}|| \leq C_3. \tag{58}$$

All Hilbert spaces of the same dimension are isomorphic and, consequently, $\boldsymbol{P}$ and $\boldsymbol{Q}$ can be represented by matrices $\in R^{m \times n}$. All matrices $\in R^{m \times n}$ are continuous. Moreover, the mappings $\boldsymbol{P}$ and $\boldsymbol{Q}$ are both linear.

All linear and continuous operators are bounded [15] and, hence, the mapping-induced finite-difference scheme of the SCN–TLM scheme is stable if the TLM algorithm is stable, which indeed, is the fact.

[3] $||\boldsymbol{\Gamma S}|| = ||\boldsymbol{\Gamma TS}||$ as the time-shift operator $\boldsymbol{T}$ is also isometric.

VII. Convergence of the Classical TLM Scheme

A. Convergence

In the last sections, we have shown that if the operating conditions of the TLM scheme are slightly changed, we can deduce mapping-induced finite-difference schemes for Johns' SCN with and without stubs. For these mapping-induced finite-difference schemes, we have analytically proven convergence using Lax's theorem.

In this section, we also want to show that this result implies the convergence of the TLM scheme under normal operating conditions.

We have shown via Lax's theorem that[4]

$$\lim_{\Delta t \to 0} ||(\boldsymbol{PT\Gamma SQ})^k \boldsymbol{f}(0) - \boldsymbol{f}(k\Delta t)|| \longrightarrow 0. \tag{59}$$

Now, we want to show that this implies

$$\lim_{\Delta t \to 0} ||\boldsymbol{P}(\boldsymbol{T\Gamma S})^k \boldsymbol{Q} \boldsymbol{f}(0) - \boldsymbol{f}(k\Delta t)|| \longrightarrow 0. \tag{60}$$

Consequently, we need to show that

$$\lim_{\Delta t \to 0} ||(\boldsymbol{PT\Gamma SQ})^k - \boldsymbol{P}(\boldsymbol{T\Gamma S})^k \boldsymbol{Q}|| \longrightarrow 0. \tag{61}$$

Applying the Schwarz inequality to (61) yields

$$\begin{aligned} &||(\boldsymbol{PT\Gamma SQ})^k - \boldsymbol{P}(\boldsymbol{T\Gamma S})^k \boldsymbol{Q}|| \\ &\quad = ||\boldsymbol{PT}^k (\boldsymbol{\Gamma SQP} - \boldsymbol{\Gamma S})^{k-1} \boldsymbol{\Gamma SQ}|| \\ &\qquad \leq ||\boldsymbol{PT}^{k-1}||||(\boldsymbol{\Gamma SQP} - \boldsymbol{\Gamma S})||^{k-1} ||\boldsymbol{T\Gamma S}||||\boldsymbol{Q}||. \end{aligned} \tag{62}$$

Obviously, all norms on the right-hand side of inequality (62) are bounded. We now need to show that one of the terms on the right-hand side of the inequality becomes arbitrarily small and constitutes an upper bound for the distance between the two schemes.

The induced norm of an operator is defined by [8]

$$||A|| = \sup_{||x|| \leq 1} ||Ax||. \tag{63}$$

We can estimate the operator norm by considering the norm of the sum of the columns, as we have a matrix representation of the operator at our hands, i.e.,

$$\sup_{||x|| \leq 1} ||Ax|| \leq \sum_j |\lambda_j| ||Ae_j||. \tag{64}$$

The λ_j denote constants. We will focus on the factor $||\boldsymbol{\Gamma SQP} - \boldsymbol{\Gamma S}||$.

In case of a TLM without stubs, we get, for $j = 1$, (65), shown at the bottom of the following page, where L, M, N is the

[4] $\Delta t \to 0$ implies $k \to \infty$ with $\lim_{k \to \infty} \Delta t_k \, k = T$, where $\{\Delta t_k\}$ is an arbitrary zero sequence.

number of TLM cells in the x-, y-, and z-directions of the computational domain, respectively. It is only summed over l, m, n [see the definition of the norm (7), (8)], as the operators $\boldsymbol{\Gamma}, \boldsymbol{S}, \boldsymbol{Q}$, and $\boldsymbol{P}$ act on $(\ell_{2,\Delta x,\Delta y,\Delta z}(\boldsymbol{G}))^{12}$. Taking the limit $l\Delta x$, $m\Delta y$ and $n\Delta z$ converge against the width of the domain in directions x, y, and z (assuming a block domain). Exploiting the fixed relation between Δl and Δt, we are left with $\sqrt{\Delta t}\, C_s$. The constant C_s denotes the squared absolute value of the shift operators in (65). The same results for all other terms and, hence, we have an upper bound of the order $\mathcal{O}(\sqrt{\Delta t})$.

B. Order of Accuracy Estimation

In the previous sections, we have shown that

$$\|(\boldsymbol{PTTSQ})^k \boldsymbol{f}(0) - \boldsymbol{f}(k\Delta t)\| \leq \mathcal{O}(\Delta t) \tag{66}$$

and

$$\|(\boldsymbol{PTTSQ})^k \boldsymbol{f}(0) - \boldsymbol{P}(\boldsymbol{TTS})^k \boldsymbol{Qf}(0)\| \leq \mathcal{O}\left(\sqrt{\Delta t}\right). \tag{67}$$

With this, we want to estimate the asymptotic convergence order of Johns' SCN–TLM scheme yielding

$$\begin{aligned}
&\|\boldsymbol{P}(\boldsymbol{TTS})^k \boldsymbol{Qf}(0) - \boldsymbol{f}(k\Delta t)\| \\
&\quad = \|\boldsymbol{P}(\boldsymbol{TTS})^k \boldsymbol{Qf}(0) - (\boldsymbol{PTTSQ})^k \boldsymbol{f}(0) \\
&\qquad + (\boldsymbol{PTTSQ})^k \boldsymbol{f}(0) - \boldsymbol{f}(k\Delta t)\| \\
&\quad \leq \|\boldsymbol{P}(\boldsymbol{TTS})^k \boldsymbol{Qf}(0) - (\boldsymbol{PTTSQ})^k \boldsymbol{f}(0)\| \\
&\qquad + \|(\boldsymbol{PTTSQ})^k \boldsymbol{f}(0) - \boldsymbol{f}(k\Delta t)\| \\
&\quad \leq \mathcal{O}(\sqrt{\Delta t}).
\end{aligned} \tag{68}$$

Surprisingly, the classical Johns TLM scheme is asymptotically only of the order of $\mathcal{O}(\sqrt{\Delta t})$, as this term dominates for small Δt!

At first sight, this appears to contradict common belief, but from the numerical studies presented in the following section, we will see that, this is, indeed, the case. We can envisage this such that not mapping between the discretized field components and the TLM wave amplitudes at each time step adds an error term with a small constant of the order $\mathcal{O}(\sqrt{\Delta t})$ to the first-order equivalent finite-difference schemes (29), (37), (39), (46), and (48), which otherwise cancels.

VIII. Numerical Verification

To verify the predictions of the previous sections, the propagation of a linearly polarized Gaussian pulsed plane wave in an axial direction of the TLM mesh was analyzed numerically.

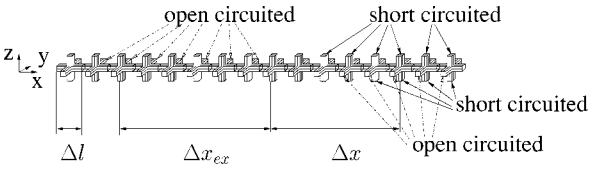

Fig. 3. TLM model of parallel-plate waveguide.

TABLE I
Parameters of Different Discretization Levels

no.	Δl_{no} [μm]	N_{no}	M_{no}
1	1.0	70	6
2	0.5	140	12
3	0.25	280	24
4	0.125	560	48
5	0.0625	1120	96
6	0.03125	2240	192
7	0.015625	4480	384

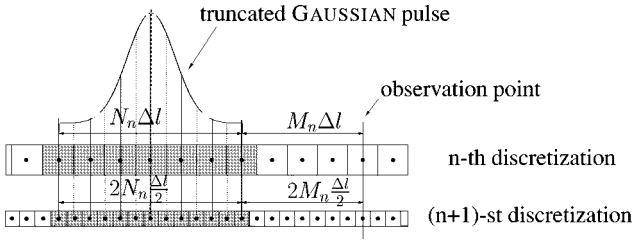

Fig. 4. TLM models for two subsequent discretization steps.

Fig. 3 shows the investigated structure. For a plane wave linearly polarized in z-direction and propagating in x-direction, a linear row with a single TLM cell in the transverse directions is representative. The ports of the TLM cells are short circuited in the z-direction and open in the y-direction. Cubic TLM cells were considered. The size of a TLM cell is Δl. The initial field is distributed across the distance Δx_{ex}. The distance between initial field and observation point is denoted Δx.

The numerical IVP was solved with various discretizations. The respective simulation parameters can be found in Table I. Fig. 4 schematically shows the TLM models for two subsequent discretization steps.

The initial field distribution, given by the discretized truncated Gaussian pulse

$$E^z_{k=1}(x) = \begin{cases} E_0 \exp\left[-\pi\left(\frac{x-x_0}{\sqrt{2\sigma}}\right)^2\right], & \text{for } x_1 \leq x - x_0 \leq x_2 \\ 0, & \text{elsewhere} \end{cases} \tag{69}$$

(with $x_1 = (N_{no}/2\Delta l_{no})$ and $x_2 = ((N_{no}/2) + 1)\Delta l_{no})$ is distributed across the distance $\Delta x_{ex} = N_{no}\Delta l_{no}$. The region,

$$\|(\boldsymbol{\Gamma SQP} - \boldsymbol{\Gamma S})e_1\| = \sqrt{\frac{(2c_0)^2\Delta t^3}{\Delta l^2}\frac{LMN}{16}\left(|2\boldsymbol{X}|^2 + |\boldsymbol{Y}^2| + |-\boldsymbol{Y}^\dagger|^2 + |-\boldsymbol{Z}|^2 + |-\boldsymbol{Z}^\dagger|^2\right)\Delta x\Delta y\Delta z} \tag{65}$$

where the initial field is given, is marked by the shaded cells in Fig. 4. The pulse is centered around $\Delta x_0 = (N_{no}/2+1)\Delta l_{no}$ (see the dashed line of Fig. 4). The width of the pulse is $\sqrt{2}\sigma = N_{no}\Delta l_{no}/p$, where p was chosen $3\sqrt{2}$.

The overall length of the structure was chosen such that, in connection with the duration of the simulation, no reflections from the terminating walls in the positive and negative x-direction occurred at the observation point. In the case with stubs, a medium with $\varepsilon_r = 2$ and $\mu_r = 1$ was assumed. In the case of a lossy medium, the electric conductivity was chosen isotropically $\sigma_e = 30\ \mathrm{Sm}^{-1}$. In this experiment, the reference solution was obtained from a simulation with very small cell size (no. 7 of Table I).

The relative error between reference solution and solutions obtained with larger cell sizes is given by

$$\eta = \sqrt{\frac{\sum_k \left(|u_k|^2\right)}{\left(|E^z_{k,\mathrm{ref}}|^2\right)}} \tag{70}$$

with

$$u_k = E^z_{k,\mathrm{ref}} - E^z_k. \tag{71}$$

A. Results

First, we want to look at the relative error η of the mapping-induced finite-difference scheme following (28), (37), (39), (46), and (48). In Fig. 5, the relative error between reference solution and solutions obtained at larger cell sizes is plotted versus the cell size normalized to the pulsewidth σ of the initial Gaussian pulse, i.e., $\Delta l_{\mathrm{norm}} = (70/3)\Delta l_{no}/\sigma$. We can clearly discern a first-order convergence rate for both the mapping-induced scheme with and without stubs. The reason why the slope of the error curve slightly increases toward the finest discretization is that the reference solution and the solution obtained at the previous discretization step are too close together.

In Fig. 6, where the relative error for Johns' classical TLM scheme is plotted versus the cell size normalized to the pulsewidth σ of the initial Gaussian pulse, we recognize a completely different behavior. Although one observes a second-order convergence for coarse discretizations, the slope of the error curve reduces toward finer discretizations very quickly. One can deduce an asymptotic convergence rate of $\sqrt{\Delta t}$ in the log–log plot of Fig. 6. As the slope of the error curve reduces at relatively fine discretization levels, which involves large mesh sizes of about $500 \times 500 \times 500$ cells, this appears to be the reason why one has not observed this reduction of the convergence rate before.

Looking more closely at Fig. 6, one observes that, in the case of TLM with stubs, the reduction of the convergence rate appears at coarser discretizations in comparison to the TLM scheme without stubs. This is due to the fact that the stubs add additional dispersion to the scheme, which further corrupts the solution, as one has no dispersion in the axial direction in a TLM mesh without stubs.

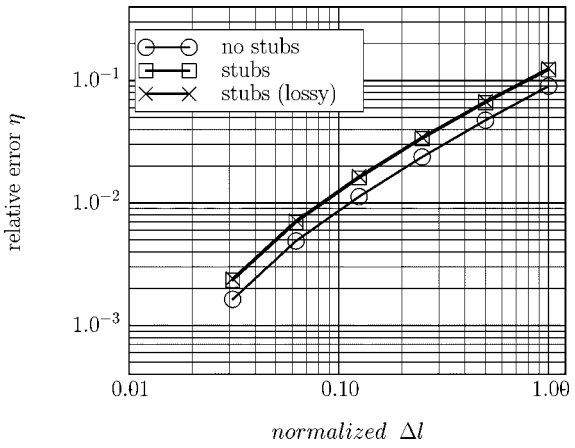

Fig. 5. Plot of relative error versus normalized cell size for a mapping-induced finite-difference scheme following (28). The normalized Δl calculates $\Delta l_{\mathrm{norm}} = (70/3)\Delta l_{no}/\sigma$.

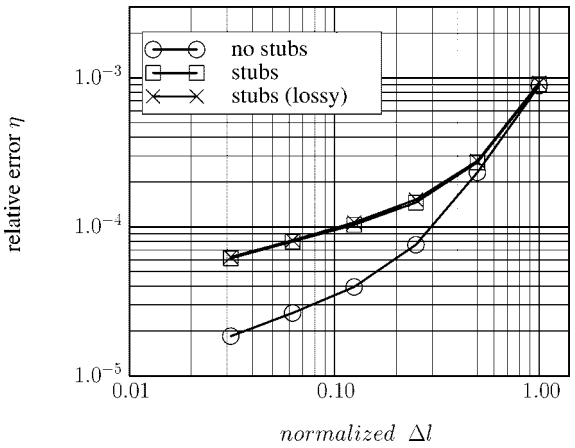

Fig. 6. Plot of relative error versus normalized cell size for a classical TLM scheme. The normalized Δl calculates $\Delta l_{\mathrm{norm}} = (70/3)\Delta l_{no}/\sigma$.

It should be remarked that the proofs of convergence presented in Section III –Section VII give statements on the *asymptotic* convergence rate. This means, a scheme with lower *asymptotic* convergence rate can yield more accurate results at certain (practical) discretization levels than a dissipative scheme within the end higher *asymptotic* convergence rate. It depends on the error constants of the scheme's error terms that vanish toward the limit $\Delta x \longrightarrow 0$ [8]. Of course, at some point, the scheme with the higher convergence order will be more accurate when the discretization becomes fine enough.

IX. Conclusion

In this paper, we have presented a proof for the convergence of Johns' original TLM scheme.

If the mappings between the discretized electromagnetic-field components and the TLM wave pulses are applied at each time step, one gets a mapping-induced finite-difference scheme, which is of first order in time in all cases. The mapping-induced finite-difference schemes are convergent due to consistency and stability. As the relation between time step and spatial increment is fixed, the first-order term is dominant and, consequently, the first-order convergence was experimentally verified.

Further, it was shown that, from the convergence of the mapping-induced finite-difference schemes, the convergence of the classical Johns TLM scheme follows. However, it emerged that asymptotically the TLM scheme using the mapping rules of Johns is only of the order $\mathcal{O}(\sqrt{\Delta t})$. The lower asymptotic convergence order has also been experimentally verified.

This means that the mapping between the discretized electromagnetic-field components and the TLM state variables plays a decisive role. Further, this result implies that the convergence order of the TLM scheme cannot simply be deduced from investigating the dispersion relation, as commonly believed.

Consequently, a formulation of the TLM scheme should be used, which uses the bijective cell-boundary-orientated mapping between the discretized electromagnetic field and TLM state variables, such as [2] and [7], as TLM schemes with this mapping indeed exhibit *second-order* convergence. In [7], the TLM scheme is constructed such that the solutions of the TLM scheme fulfill a consistent second-order finite-difference scheme. In this formulation, the fields are sampled at the boundary, and at the cell center the fields are the average of the field components at the boundary. In [16], we numerically compared the convergence of these different TLM formulations.

ACKNOWLEDGMENT

The authors wish to express thanks to T. Mangold, Institut für Hochfrequenztechnik, Technische Universität München, Munich, Germany, for many fruitful discussions.

REFERENCES

[1] P. B. Johns, "A symmetrical condensed node for the TLM method," *IEEE Trans. Microwave Theory Tech.*, vol. MTT-35, pp. 370–377, Apr. 1987.

[2] M. Krumpholz and P. Russer, "A field theoretical derivation of TLM," *IEEE Trans. Microwave Theory Tech.*, vol. 42, pp. 1660–1668, Sept. 1994.

[3] H. Jin and R. Vahldieck, "Direct derivations of TLM symmetrical condensed node and hybrid symmetrical condensed node from Maxwell's equations using centered differencing and averaging," *IEEE Trans. Microwave Theory Tech.*, vol. 42, pp. 2554–2561, Dec. 1994.

[4] Z. Chen, M. M. Ney, and W. J. Hoefer, "A new finite-difference time-domain formulation and its equivalence with the TLM symmetrical condensed node," *IEEE Trans. Microwave Theory Tech.*, vol. 39, pp. 2160–2169, Dec. 1991.

[5] M. Aidam and P. Russer, "Derivation of the transmission line matrix method by finite integration," *Arch. Elektr. Ubertragung*, vol. 51, no. 1, pp. 35–39, Jan. 1997.

[6] J. LoVetri and N. R. S. Simons, "A class of symmetrical condensed node TLM methods derived directly from Maxwell's equations," *IEEE Trans. Microwave Theory Tech.*, vol. 41, pp. 1419–1428, Aug. 1993.

[7] S. Hein, "Consistent finite-difference modeling of Maxwell's equations with lossy symmetrical condensed node," *Int. J. Numer. Modeling*, vol. 6, pp. 207–220, 1993.

[8] J. W. Thomas, *Numerical Partial Differential Equations*. Berlin, Germany: Springer-Verlag, 1995.

[9] E. Zeidler, *Applied Functional Analysis*. Berlin, Germany: Springer-Verlag, 1995.

[10] ——, *Nonlinear Functional Analysis and Its Applications II/B*. Berlin, Germany: Springer-Verlag, 1985.

[11] R. D. Richtmyer, *Principles of Advanced Mathematical Physics*. Berlin, Germany: Springer-Verlag, 1978.

[12] P. Russer and M. Krumpholz, "The Hilbert space formulation of the TLM method," *Int. J. Numer. Modeling*, vol. 6, no. 1, pp. 29–45, Feb. 1993.

[13] P. A. M. Dirac, *The Principles of Quantum Mechanics*. Oxford, U.K.: Oxford Univ. Press, 1958.

[14] P. Naylor and R. A. Desai, "New three dimensional symmetrical condensed lossy node for solution of electromagnetic wave problems by TLM," *Electron. Lett.*, vol. 26, no. 7, pp. 492–495, Mar. 1990.

[15] L. Debnath and P. Mikusiński, *Introduction to Hilbert Spaces with Applications*. New York: Academic, 1990.

[16] J. Rebel, M. Aidam, and P. Russer, "A numerical study on the accuracy of TLM–SCN formulations for the solution of initial value problems," in *15th Annu. Rev. Progress Appl. Comput. Electromag. Dig.*, 1999, pp. 628–635.

Jürgen N. Rebel was born in Munich, Germany, in 1971. He received the Dipl.-Ing. degree in electrical engineering and information technology and the Dr.-Ing. degree in RF technology from the Technische Universität München, Munich, Germany, in 1997 and 2000, respectively. His doctoral research concerned theoretical and experimental convergence analyses of various formulations of the TLM method.

Since 2000, he has been with the Wireless Group, Infineon Technologies AG, Munich, Germany.

Martin Aidam received the Dipl.-Ing. degree from the Technische Universität Berlin, Berlin, Germany, in 1995, and the Dr.-Ing. degree from the Technische Universität München, Munich, Germany, in 2000.

From 1995 to 1999, he was with the Lehrstuhl für Hochfrequenztechnik, Technische Universität München. In 1999, he joined DaimlerChrysler, where he is currently involved in the area of electromagnetic compatibility. His research has focused on electrostatic discharges and numerical methods for solving electromagnetic field problems, in particular, boundary integral methods, the TLM method, and wavelet-based schemes in time domain.

Peter Russer (SM'81–F'94) received the Dipl.-Ing. and Dr. Techn. degrees from the Technische Universität Wien, Vienna, Austria, in 1967 and 1971, respectively, both in electrical engineering.

From 1968 to 1971, he was an Assistant Professor with the Technische Universität Wien. In 1971, he joined the Research Institute, AEG-Telefunken, Ulm, Germany, where he was involved with fiber-optic communication, broad-band solid-state electronic circuits, statistical noise analysis of microwave circuits, laser modulation, and fiber optic gyroscopes. Since 1981, he has been a Professor and Head of the Institut für Hochfrequenztechnik, Technische Universität München, Munich, Germany. In 1990, he was a Visiting Professor at the University of Ottawa, Ottawa, ON, Canada. In 1993, he was a Visiting Professor at the University of Victoria, Victoria, BC, Canada. From October 1992 to March 1995, he was Director of the Ferdinand-Braun-Institut für Hochstfrequenztechnik, Berlin, Germany. He has authored or co-authored over 300 scientific papers. His current research interests are electromagnetic fields, integrated microwave and millimeter-wave circuits, statistical noise analysis of microwave circuits, and methods for computer-aided design of microwave circuits. He is an Editorial Board member for *Electromagnetics* and the *International Journal of Numerical Modeling*. He is co-chairman of the International Scientific Radio Union (URSI) Commission D.

Dr. Russer is member of the German Informationstechnische Gesellschaft (ITG) and the German as well as Austrian Physical Societies. He has served as a member of the Technical Program Committees and Steering Committees of various international conferences, including those of the IEEE Microwave Theory and Techniques Society (IEEE MTT-S) and European Microwave Conference. He was a corecipient of the 1979 Nachrichtentechnische Gesellschaft (NTG) Award for his paper "Electronic Circuits for High Bit Rate Digital Fiber Optic Communication Systems."